scientific reports

Check for updates

OPEN

Vitiligo detection capabilities of 1D photonic crystal biosensing design

Ali S. Alshomrany[1], Arafa H. Aly[2,8]✉, B. A. Mohamed[2], S. Alamri[3,4], D. Mohamed[2], S K Awasthi[5], Zinab. S. Matar[6], A F Amin[7] & H. Hanafy[2]

This theoretical work focuses on the application of Tamm resonance-based biosensing using a one-dimensional photonic crystal for detecting skin vitiligo, a condition caused by the loss of pigment in the body. This biosensor utilizes the interaction of light with the photonic structure to identify the specific biomarkers associated with vitiligo. The proposed structure is composed of prism/Ag/skin-sample/$(GaP/PS)^N$/glass. The MATLAB simulations are used to obtain numerical results pertaining to the work by using the transfer matrix method (TMM). The analysis of transmission spectra of the proposed structure shows its minute sensing ability of detecting skin vitiligo. The proposed sensor possesses a higher sensitivity of 1200 nm/RIU which is higher than the sensitivities of the sensor reported earlier. Moreover, the suggested biosensor possesses an extremely high-quality factor value of 40,650 with an exceptionally small *full-width-half-maximum* value of 0.04 nm.

Keywords Biosensor, Photonic Crystal, Refractive index (RI), Sensitivity, Vitiligo, Surface plasmon resonance (SPR).

Vitiligo is a skin disorder characterized by the loss of pigment-producing cells, which results white patches on the skin[1]. This disorder, which is physically disfiguring, particularly in dark-skin people, renders the lesion skin more vulnerable to sunburn. Almost 0.1 to 2% of the global population, regardless of race or gender is affected with this skin disorder[2]. Various mechanisms, such as genetic, inflammatory, autoimmune, oxidative, and metabolic changes, are responsible for melanocyte loss in vitiligo; but the response of individual's body with these alterations are still debatable[3]. In general, this condition is caused by a loss or reduction in the pigments that exist in human skin, which are important in maintaining skin color regardless of pollution and the area of the skin exposed with sunlight. Some of the pigments that lead to vitiligo include: Melanin, Keratin, Collagen, Dermis and Epidermis[4]. An optical biosensor based on photonic crystal may be one of the potential methods for detecting and diagnosing vitiligo[5]. Such biosensors utilize the principles of light interaction with the photonic structures to detect specific biomarkers associated with vitiligo. The selective capturing followed by detection of these biomarkers may provide an opportunity of it's rapid and accurate diagnosis to prevent the disease[6]. Photonic technology has potential to revolutionize the diagnosis and monitoring of vitiligo by providing a non-invasive and efficient method to healthcare professionals. Any futuristic advancement in vitiligo detection and its diagnosis could significantly address the worries of the patient which improves our understanding of the underlying mechanisms related to the disorder. In recent years photonic crystals (PCs) have received lot of attention from both industries and academic institutions because of their applications in photonics, biochemistry, and electronics[7]. PCs belong to recent category of materials in which refractive index (RI) varies periodically in one-dimension (1D), two-dimensions (2D), and three-dimensions (3D)[8]. When light waves hit the PC, certain photons are permitted to pass through them while others are forbidden (completely reflected). The forbidden photons lying within specific wavelength range lead to the appearance of stop bands in the transmission spectrum that is commonly referred to a as photonic band gap (PBG)[9]. Consequently, PC offers amazing control over light propagation which allows them to be used in designing of integrated optical devices[10–12]. Recently, fundamentals of photonics are integrated with plasmonic for the development of new kind of photo-plasmonic sensing devices for detection of minute change in environmental refractive index (RI). Such new type of photo-photonic devices have intriguing capability of enhancing the light matter interaction

[1]Department of Physics, College of Sciences, Umm Al-Qura University, Al Taif HWY, Mecca 24381, Saudi Arabia. [2]Physics Department, Faculty of Sciences, TH-PPM Group, Beni-Suef University, Beni Suef 62514, Egypt. [3]Department of Mechanical Engineering, College of Engineering, King Khalid University, Abha 62529, Saudi Arabia. [4]Center for Engineering and Technology Innovations, King Khalid University, Abha 61421, Saudi Arabia. [5]Department of Physics and Material Science and Engineering, Jaypee Institute of Information Technology, Noida 201304, U.P, India. [6]Physics Department, College of Science, Umm Al-Qura University, Makkah, Saudi Arabia. [7]Faculty of Technology and Education, Beni-Suef University, Beni Suef 62111, Egypt. [8]Higher Technological Institute of Applied Sciences in Beni-Suef (HSI), Beni Suef, Egypt. ✉email: arafa.hussien@science.bsu.edu.eg; arafaaly@aucegypt.edu

which yields single photon emission, biosensors and lasers. The excitation of electromagnetic radiation (ER) at the interface between the plasmonic metal (like gold and silver) and 1D PC is responsible for Tamm resonance (TR) which is also known as Tamm plasmon polariton (TPP). Photo-plasmonic devises can excite Tamm resonance irrespective of polarization state of incident light corresponding to any incident angle. Unlike surface plasmon resonance (SPR) based plasmonic sensors Photo-plasmonic devices do not require a diffractive grating or prim to couple light into the structure. Additionally, in SPR biosensors excitation of ER is possible at a specific angle corresponding to TM polarized wave only. Photo-plasmonic structures have special ability of excitation of Tamm resonance corresponding to both polarization states in without requiring any kind of prism coupler. From last two decades photo-plasmonic biosensing provides an opportunity of real-time and label-free detection of biomolecular interactions[13]. Tamm resonance yields confinement of ER at the interface between the 1D PC and the metallic layer, resulting in the appearance of a sharp peak within the PBG[14]. The position of this peak is extremely sensitive to the optical characteristics of the PC and its surroundings[15]. Hence, such structure can be employed to design sensors. In this paper we have theoretically investigated Tamm resonance based one-dimensional photonic crystal for detection of vitiligo. The results of the proposed work are carried out transfer matrix method (TMM) based MATLAB simulations.

Architecture of proposed biosensor and theoretical model

The proposed photonic biosensor based on Tamm resonance is composed of 1D PC as depicted in Fig. 1. The proposed design [Prism/Ag/skin-sample/$(GaP/PS)^N$/glass substrate] is realized by associating glass prism with 1D PC [$(GaP/PS)^N$/glass substrate] through thin and thick layers of silver (Ag) and air respectively. The thick hollow layer of air is used as cavity to infiltrate the vitiligo-infected skin samples under investigation. The binary 1D PC [$(GaP/PS)^N$/glass substrate] is made up of Gallium phosphide (GaP) and porous silicon (PS) layers deposited one over the other by repeating the pair of GaP and PS layers N times. The entire structure is deposited over glass substrate as shown in Fig. 1. The period number N of the structure is optimized to 10. The optimization of the period number of the photonic sensor is done in a way to get wider PBG so that TPP mode can be allowed to move inside PBG depending upon the nature of the sample poured into the cavity. Additionally, it also allows us to increase the number of skin samples to be examined. The application of prism is preferred due to variety of reasons to couple light into the optical systems. (1) Its capability of changing the direction of propagation of light entering into the system, (2) for creating dispersion to separate the light into different elements, (3) due to optic rarities, (4) It can also change the polarization of light and (5) To produce veritably important hindrance pattern which are useful in PCs. The refractive indices of the prism material, GaP, and PS layers are 2.5[16], 3.32[17] and 1.56[18], respectively. The thickness of thin Ag layer (d_m) is kept as 25 nm. In addition, the thicknesses of the sensing region of air, GaP and PS layers are taken as $d_s = 700$ nm, $d_1 = 250$ nm and $d_3 = 435$ nm respectively. The refractive index (RI) of thin metallic layer of Ag is calculated by using Drude model as[19,20].

$$n_{Ag} = \sqrt{1 - \frac{\omega_p^2}{(\omega^2 + i\gamma\omega)}} \tag{1}$$

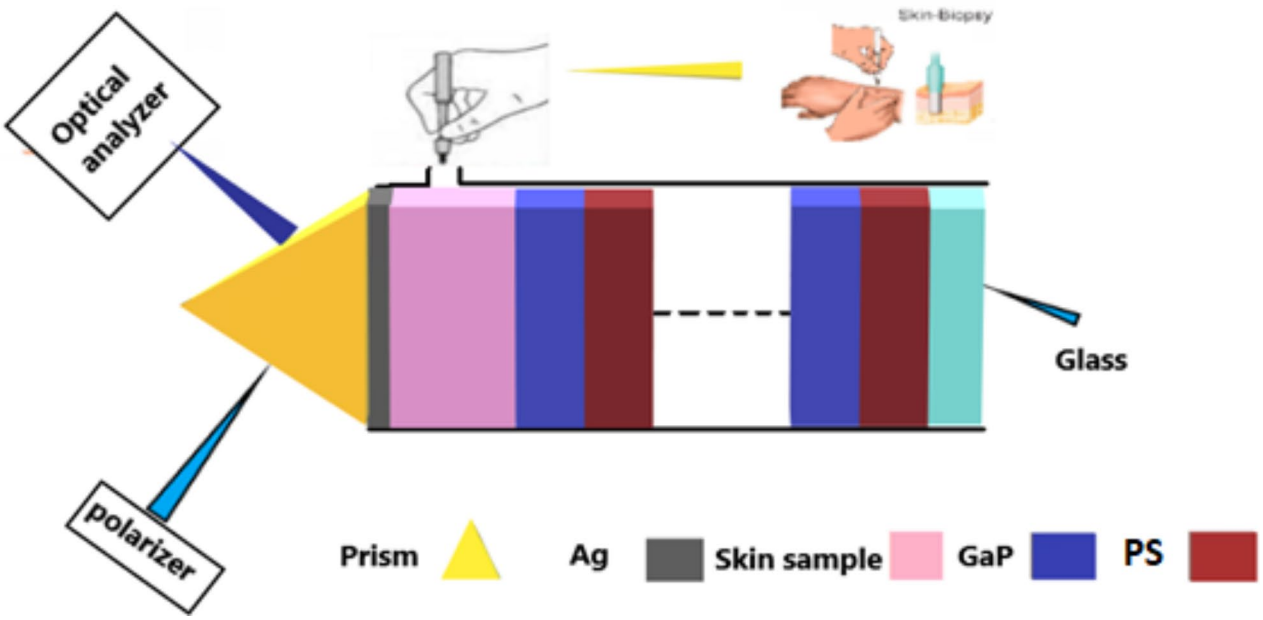

Fig. 1. Schematic diagram of proposed sensor composed of Prism/Ag/Skin-Sample/$(GaP/PS)^N$/Glass. Here yellow, gray, orange, blue, maroon and cyan coloured regions are representing prim, metallic layer, sensing region filled with skin sample, GaP layer, PS layer and glass substrate of the design respectively.

Here ω_p (= 2.18 PHz), γ (= 4.353 THz) and ω are representing plasma frequency, damping factor associated with Ag and frequency of incident radiation respectively.

The sensing and detection capabilities of the proposed sensor are examined by investigating the transmission characteristics of the biosensor, simulated by MATLAB computational software in the light of transfer matrix method (TMM). The description of typical TMM is given as[15,21–23].

$$\mathbb{N} = \begin{pmatrix} \mathbb{N}_{11}; & \mathbb{N}_{12} \\ \mathbb{N}_{21}; & \mathbb{N}_{22} \end{pmatrix} = (\mathrm{I}_m)\,(\mathrm{I}_S)\;\mathrm{I}_A\mathrm{I}_B \tag{2}$$

where I_m, I_S, I_A *and* I_B are the transfer matrices representing metallic layer, sensing medium, GaP and PS layers respectively. The elements of the entire 2 × 2 transfer matrix $\mathbb{N}$ are represented by $\mathbb{N}_{ij}$ (i = 1 to 2 and j = 1 to 2). The characteristic matrix of any layer j of the biosensor can be defined as[21]

$$I_j = \begin{bmatrix} \cos(_j) & -iD_j^{-1}\sin(_j) \\ -iD_j\sin(_j) & \cos(_j) \end{bmatrix} \tag{3}$$

Here $?_j = \frac{2\pi\, d_j}{\lambda}\; n_j\, cos(\theta_{\,j})$ is defined as the phase difference between incoming and outgoing light waves inside j^{th} layer of the structure (j = m, sample, A, B, and substrate)[22]. The $symbol\ \lambda$ is used for representing free space wavelength of incident light, d_j is the thickness of j^{th} layer, n_j is the j^{th} layer's refractive index. The $\theta_{\,j}$ is the refracted angle inside j^{th} layer which is related to the incident angle $\theta_{\,o}$ as[23]

$$cos(\theta_{\,j}) = \sqrt{1 - \left(\frac{n_o\, cos(\theta_{\,o})}{n_j}\right)^2} \tag{4}$$

and $?_j = n_j\, cos(\theta_{\,j})$ for transverse electrical (TE) waves, whereas $?_j = cos(\theta_{\,j})/\, n_j$ for transverse magnetic (TM) waves. The surrounding medium's refractive index is represented by n_o[23]. The symbols $\theta_{\,0}, \theta_{\,m}, \theta_{\,sam}, \theta_{\,A}, \theta_{\,B}$, and $\theta_{\,substrate}$ are used to represent propagation angles of incident in prism, metal (Ag), sample, GaP, PS, and substrate respectively.

The transmission coefficient (t)[24] and the transmittance (T)[25] of the biosensor is computed as

$$t = \frac{2D_o}{D_oN_{11} + D_oD_tN_{12} + N_{21} + D_tN_{22}} \tag{5}$$

$$t = \frac{D_t}{D_o}\;|t|^2 \tag{6}$$

Here symbols $?_{\mathrm{o}} = \mathrm{n_o}\cos(\theta_{\,\mathrm{o}})$ and $?_{\mathrm{t}} = \mathrm{n_t}\cos(\theta_{\,\mathrm{t}})$ are used to show initial and final media corresponding to TE wave[25].

The most significant parameter used to measure the performance of the suggested structure is sensitivity (S). The sensitivity is defined as the change in central wavelength of Tamm resonant mode inside PBG due to corresponding change in refractive index of the sensing medium. Mathematically, it is defined as[26]

$$\mathrm{S} = \frac{\Delta\,\lambda}{\Delta\,\mathrm{n}} \tag{7}$$

Several more parameters like quality and accuracy of the sensor are also evaluated to include various aspects of the sensing into consideration which determines the performance of the sensor. The ability of any optical sensor having narrow bandwidth is determine in terms of its quality factor (Q-Factor). Mathematically, it is defined as[27]

$$\mathrm{Q-Factor} = \frac{\lambda}{FWHM} \tag{8}$$

Here full-width-half-maximum (FWHM) = $\Delta\,\lambda_{\frac{1}{2}}$ is the difference between the wavelengths at left and right edges of Tamm resonant peak at which transmittance falls to 50% either side of the resonant peak[28].

Results and discussions

This section deals with the study of transmission spectra of the proposed structure obtained from the MATLAB simulations with the help of TMM as discussed in previous session. The interpretation of such spectra of the proposed structure loaded with the sample under investigation is used for detection of vitiligo. Figure 2 depicts the transmittance spectra of designs (*i*) prism/skin-sample/$(\mathrm{GaP/PS})^N$/glass-substrate without Ag layer and (*ii*) prism/Ag/skin-sample/$(\mathrm{GaP/PS})^N$/glass-substrate with Ag layer shown in blue and red solid line curves respectively. In both situations sensing medium is loaded with normal skin sample of refractive index 1.42. As it is evident from Fig. 2, that the absence of the metallic layer (Ag layer) results photonic-band-gap (PBG) extending from 1606 nm to 1650 nm due to the periodicity of the structure without having any transmission peak inside PBG shown in blue colour. The insertion of the metal layer (Ag) on the top of the structure via a hollow air-cavity infiltrated with normal skin sample of width 700 nm results a sharp Tamm resonant peak of transmittance 97.6% centered at wavelength 1626.5 nm inside PBG due to the phenomenon of Tamm plasmon resonance (TPR) which arises due to presence of an additional metallic layer in front of the PC via an air-cavity

Sample details	Refractive index (RI)
Epidermis	1.34
Dermis	1.41
Normal skin	1.42
Collagen	1.43
Keratin	1.51
Melanin	1.72

Table 1. Details of various vitiligo-affected cells along with their refractive indices[4].

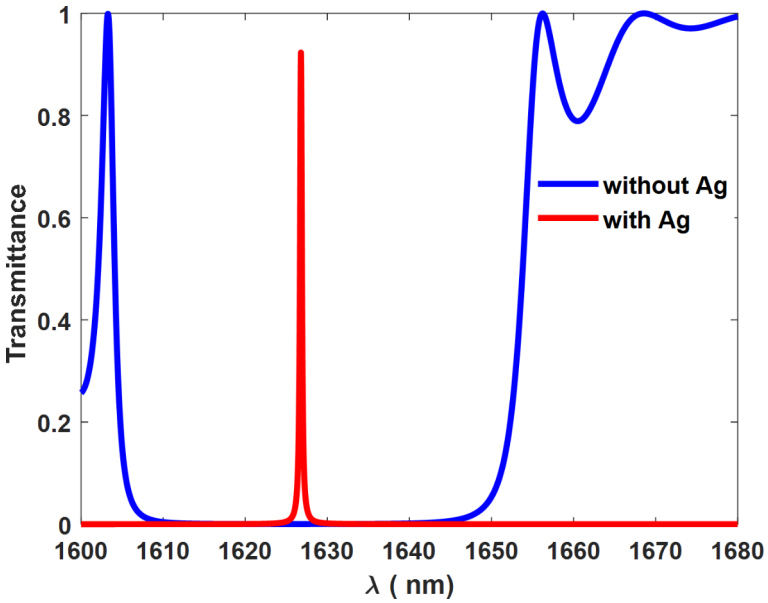

Fig. 2. Transmittance spectra of the proposed designs under normal incidence loaded with normal skin sample of refractive index 1.42 (*i*) prism/skin-sample/$(GaP/PS)^N$/glass-substrate without Ag layer and (*ii*) prism/Ag/skin-sample/$(GaP/PS)^N$/glass-substrate with Ag layer shown in blue and red solid line curves respectively. The thickness of different layers of the structure are $d_m = 25$ nm, $d_{sm} = 700$ nm, $d_1 = 250$ nm, and $d_2 = 435$ nm. The period number N of the structure is equal to 10. The hollow cavity is infiltrated with of the normal skill sample of refractive index 1.42.

region. The central wavelength of the resonance peak arises due to TPR shown by red colour solid line curve inside PBG. This TPR is extremely sensitive to the change in the effective refractive index of the design, due to change in the refractive index of the sample poured into the cavity region of the structure under investigation.

The proposed structure can identify the various types of vitiligo by detecting the minute change in the refractive index of the sample containing vitiligo-affected cells due to specific pigment loss by the body of the affected person with respect to the sample containing normal skin cells. Table 1 lists five types of the pigments cause vitiligo due to their production losses along with their corresponding refractive indices with respect to normal skin. These five types of pigments are melanin, keratin, collagen, dermis and epidermis.

Next, samples containing normal skin cells and vitiligo-infected cells due to the loss of melanin, keratin, collagen, dermis and epidermis pigments are poured into the cavity of the proposed structure one by one and the corresponding change in the positions of TPR modes inside PBG are recorded with the help of their respective transmission spectra as shown in Fig. 3 below.

It is evident from Fig. 3 that separate loading of the structure with the samples containing dermis and epidermis pigments one by one results the left shifting of TPR modes inside the PBG shown in yellow and green coloured solid line curves respectively with respect to TPR peak of the structure loaded with normal sample. This left shifting of TPR peaks is due to the decrease in the refractive index of the sample containing epidermis and dermis pigments from 1.42 corresponding to normal sample to 1.34 and 1.41 respectively. On the other hand, transmission response of the design loaded with the samples containing collagen, keratin and melanin pigments separately results the shifting of their respective TPR modes toward right inside PBG with respect to the TPR mode of the structure loaded with normal sample. TPR modes corresponding to the samples containing collagen, keratin and melanin pigments separately are shown in red, pink and blue coloured solid line curves respectively in Fig. 3 whereas the TPR mode due to normal sample is shown in black colour. The right shifting of TPR modes inside PBG is due to the increase in the refractive index of the samples containing collagen, keratin

and melanin pigments from 1.42 corresponding to normal sample to 1.43, 1.52 and 1.72 respectively. The central wavelengths of TPR modes corresponding to the samples containing epidermis, dermis, normal, collagen, keratin and melanin cells separately loaded into the cavity of the structure are 1622 nm, 1626 nm, 1626.5, 1627.5 nm, 1631 nm and 1640 nm respectively as obtained from Fig. 3. The graphical relationship between the central wavelengths of respective TPR modes arise due to various samples loaded into the cavity of the structure under investigation and their refractive indices is shown in Fig. 4. Almost linear relationship is obtained between the refractive index of the sample and the wavelength of the TPR peak, indicating that the central wavelength of the TPR peak is directly proportional to the refractive index of the sample under consideration.

Transmittance spectra shown in Fig. 5 indicates that the change in the position of central wavelength of TPR mode inside the PBG of the structure loaded with samples containing melanin pigments with respect to the sample containing normal cells shown in blue and black coloured solid line curves respectively. The intensity of the TPR mode corresponding to the sample containing melanin pigment is reduced due to loss of energy inside sample containing melanin pigments as compared to the TPR mode due to sample containing normal skin. As we can see, there is a shift of approximately 13.5 nm in the position of the central wavelength TPR modes due to change in the refractive indices of the samples poured into the cavity containing melanin pigments and normal cells separately. The shift in the position of the central wavelength of TPR modes corresponding to melanin sample with respect to normal skin is toward the higher wavelength side in addition to the reduction in the intensity of the TPR mode due to infected cell as compared to normal cell.

Next, the structure is loaded with samples containing normal skin cells and collagen pigmentation one by one to study the effect of this change on the respective TPR modes in transmission spectra shown in blue and orange coloured solid line curves inside PBG as shown in Fig. 6. It is evident from the Fig. 6 that the shift of 1 nm between the central wavelengths of TPR modes corresponding to the sample containing normal skin cells and collagen pigmentation is observed due to the increase in the refractive index of the sample containing collagen pigmentation with respect to sample containing normal cell. Though the intensity of both the TPR modes remains almost same due to minute difference in the refractive indices of both the samples. The movement of the TPR mode is towards the higher wavelength side is due to the increase in the refractive index of the sample containing collagen pigmentation with respect to normal cell. Moreover, FWHM of each TPR peak is also remain same.

After investigating the response of proposed biosensor for detecting collagen pigmentation sample with respect to the normal sample, we have investigated the sensing and detection capabilities of the structure loaded with sample containing keratin pigmentation with respect to normal sample. The transmittance response of the proposed structure loaded sample containing keratin pigmentation with respect to normal sample is shown in Fig. 7 below. It shows two TPR modes corresponding to the samples containing normal cells and keratin pigmentation cells loaded separately into the cavity region of the structure. The position of the TPR mode corresponding to normal cell shown in blue colour is shifted to higher wavelength side and acquires new position which is 4.5 nm away from the earlier position as shown in the Fig. 7 by purple colour.

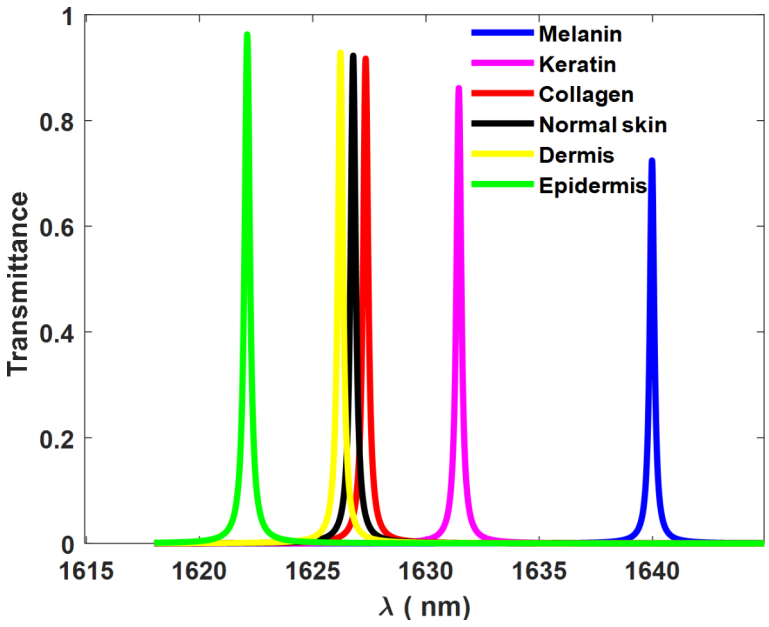

Fig. 3. Transmittance spectra of photonic design prism/Ag/skin-sample/$(GaP/PS)^N$/glass-substrate loaded with samples containing normal skin cells and vitiligo-infected cells due to the loss of melanin, keratin, collagen, dermis and epidermis pigments respectively, showing solid line TPR peaks in black, pink, red, yellow and green colours respectively under normal incidence. The period number and cavity thickness of the structure are $N = 10$ and $d_{sm} = 700$ nm respectively.

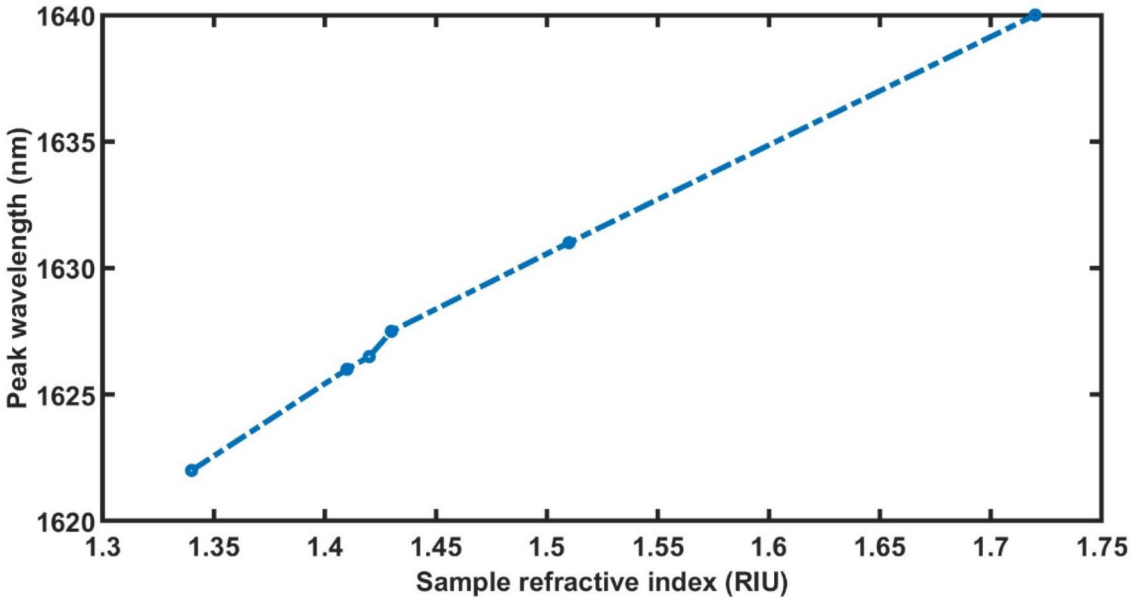

Fig. 4. Illustration of graphical relationship between the central wavelengths of the TPR modes of the sensor loaded separately with samples containing epidermis, dermis, normal, collagen, keratin and melanin cells under normal incidence with $d_{sm} = 700$ nm and $N = 10$ periods.

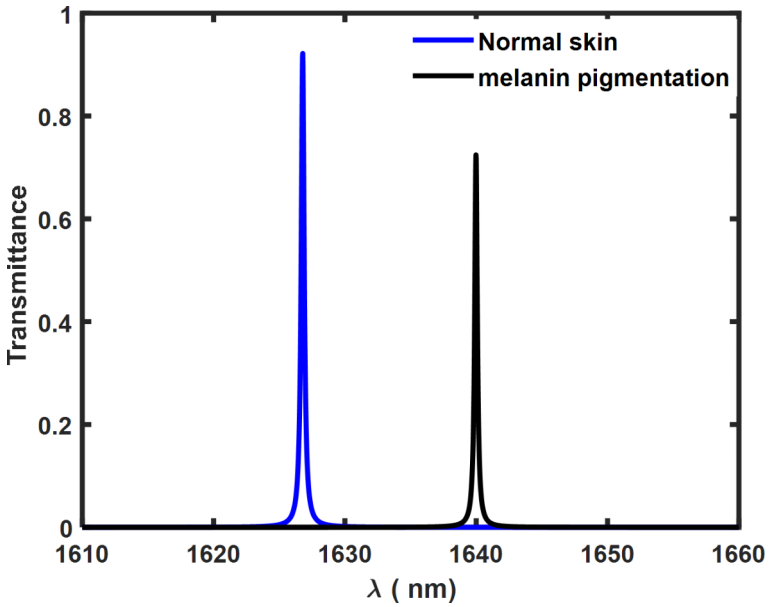

Fig. 5. Transmittance spectra showing two TPR modes of photonic design [prism/Ag/skin-sample/$(GaP/PS)^N$/glass-substarte] loaded with sample containing normal skin cells and melanin pigments shown in blue and black coloured solid line curves respectively under normal incidence with $d_{sm} = 700$ nm and $N = 10$ periods.

Next, behavior of the proposed biosensor loaded with sample containing dermis pigmentation with respect to the normal sample is examined with the help of its transmission response as shown in the Fig. 8 below. It shows blue and green coloured TPR modes corresponding to sample containing normal cells and dermis pigmentation respectively. It is observed from the Fig. 8 that the TPR mode position of the structure loaded with sample containing dermis pigmentation shifts to left of the peak corresponding to normal sample. This shift is 0.5 nm earlier inside PBG with respect to previous peak. The change in the intensity of these TPR modes is negligible as depicted.

Finally, we have examined the behavior of our biosensor loaded with the sample containing epidermis pigmentation with respect to the normal sample. For this purpose, transmission response of the structure loaded

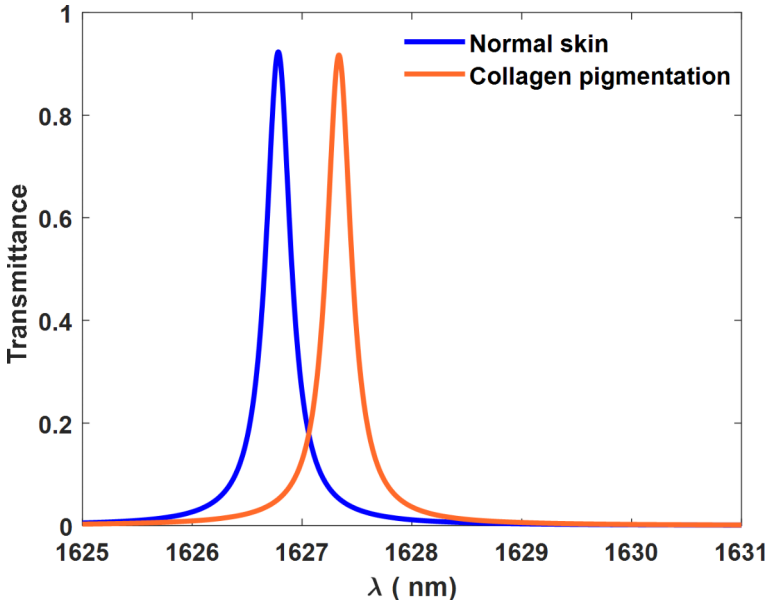

Fig. 6. Transmittance spectra shown in blue and orange coloured solid line curves of photonic design [prism/Ag/skin-sample/$(GaP/PS)^N$/glass-substrate] loaded with sample containing normal skin cells and collagen pigmentation under normal incidence for the structure with $d_{sm} = 700$ nm and $N = 10$ periods.

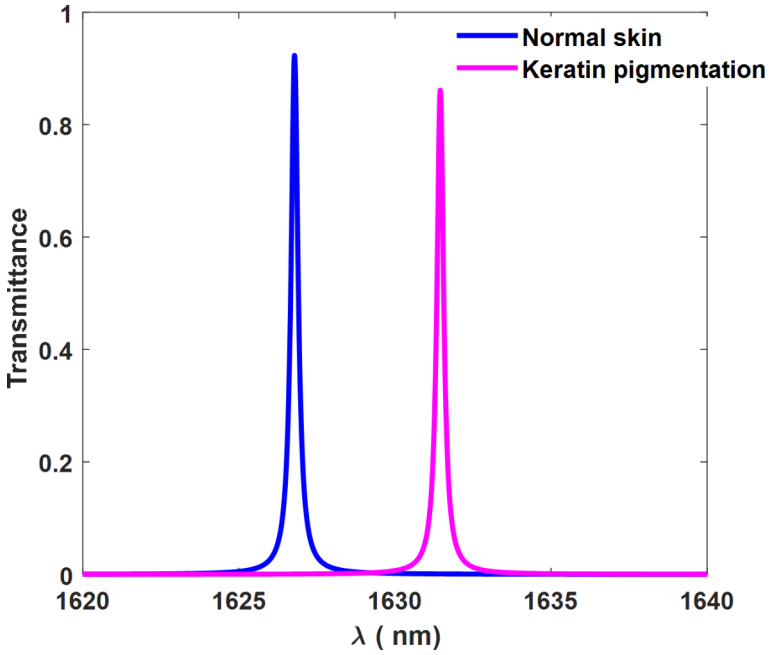

Fig. 7. Transmittance spectra containing two TPR modes shown in blue and purple colour solid lines of photonic design [prism/Ag/skin-sample/$(GaP/PS)^N$/glass-substrate] loaded with sample containing normal skin cells and keratin pigmentation respectively under normal incidence with $d_{sm} = 700$ nm and $N = 10$ periods.

with normal sample and sample containing epidermis pigmentation is obtained as depicted in Fig. 9. It contains two TPR peaks shown in blue and purple colours inside PBG of the structure loaded with normal sample and sample containing epidermis pigmentation respectively. The change in the sample containing normal cells with respect to epidermis pigmentation loaded into the cavity of the structure results the movement of TPR mode corresponding to epidermis pigmentation towards lower wavelength side. This shifting relocates the TPR mode at position inside PBG which is at the distance 4.5 nm away from the position of earlier TPR peak corresponding to normal cell. This movement results reduction in the intensity of TPR mode corresponding to epidermis

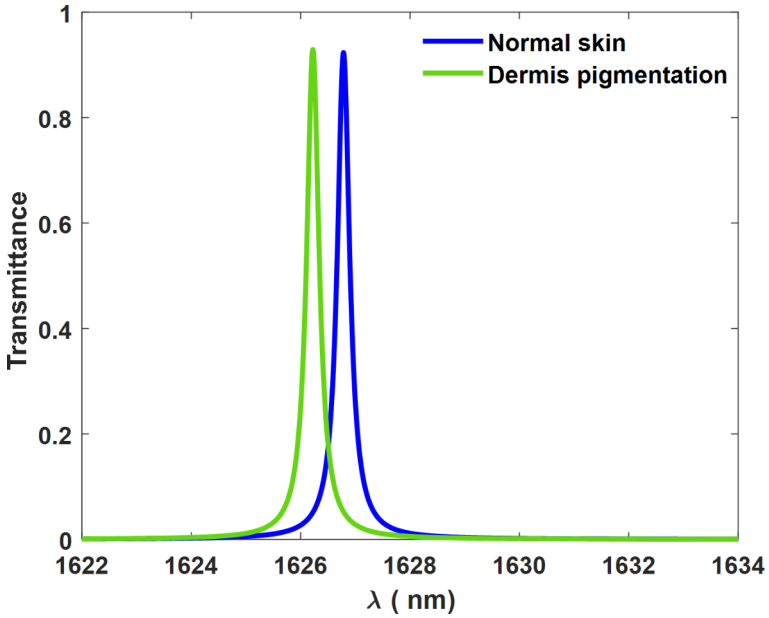

Fig. 8. Transmittance spectra shows two TPR modes in colours blue and green inside PBG of photonic design [prism/Ag/skin-sample/$(GaP/PS)^N$/glass-substrate] loaded with sample containing normal skin cells and dermis pigmentation respectively under normal incidence for the structure with $d_{sm} = 700$ nm and $N = 10$ periods.

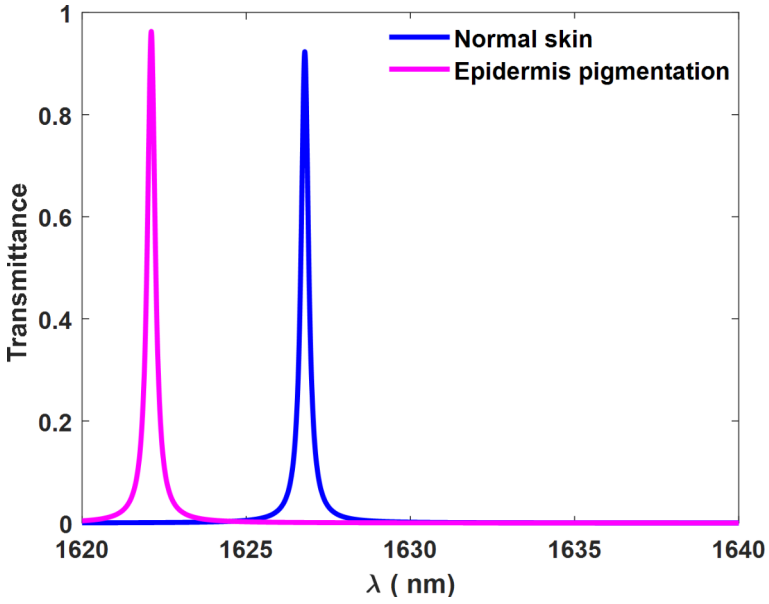

Fig. 9. Transmittance spectra shows two TPR modes in colours blue and purple inside PBG of photonic design [prism/Ag/skin-sample/$(GaP/PS)^N$/glass-substrate] loaded with sample containing normal skin cells and epidermis pigmentation respectively under normal incidence for the structure with $d_{sm} = 700$ nm and $N = 10$ periods.

pigmentation with respect to normal cell. This reduction in the intensity of TPR mode is very high as compared to the detection limit of the sensor used in the design.

Next, efforts have been given to study how change in the thickness of the cavity region affects the sensitivity of the structure loaded with dermis pigmentation with respect to normal sample. For this purpose, we have calculated sensitivity of various structures of different cavity layer thicknesses loaded with sample containing dermis pigmentation as defined in Eq. (7). The calculated sensitivity values of the structures of different cavity thicknesses loaded with sample containing dermis pigmentation with respect to the normal sample are depicted in Fig. 10 below. It can be observed from Fig. 10 that as we randomly increase the thickness of the cavity layer of

the structure from 700 nm to 5×10^3 nm, 10×10^3 nm, 15×10^3 nm, 20×10^3 nm, 25×10^3 nm and 30×10^3 nm, sensitivity of the structure initially increases and reaches to quasi-constant state upto a specific range of sample layer thickness, beyond the sample layer thickness of $d_{sm}=25\times10^3$ nm, the TRP mode moves out of PBG. Thus, the proposed structure attains maximum sensitivity corresponding to cavity layer thickness $d_{sm}=25\times10^3$ nm.

Furthermore, the effect of changing the angle of TE polarized incident light on sensitivity of the structure with cavity layer thickness $d_{sm}=25\times10^3$ nm is investigated. Figure 11 is plotted for studying the effect of change in the angle of incidence of TE polarized light on the sensitivity of the structure having $d_{sm}=25\times10^3$ nm loaded with dermis pigmentation. According to the relationship depicted in Fig. 11, the structure's sensitivity remains constant when the angle of incidence is varied from 0°to 20°, and then increases subsequently as angle of incidence increases from 20°to 65° which reaches to maximum at an angle 65°.

Finally, we have examined the sensing and detection capabilities of our structure with $d_{sm}=25\times10^3$ nm and $N=10$ at angle of incidence 65° by evaluating the FWHM, sensitivity and Q factor values of the proposed design separately loaded with all samples with respect to normal sample. For calculating the sensitivity and Q-factor values of the loaded structures we have used Eq. (7) to (8) in addition to Fig. (5) to (9) as listed in Table 2. Here it should be noted that we have taken normal skin as a reference sample.

After evaluating the performance of the proposed structure corresponding to $d_{sm}=25\times10^3$ nm and $N=10$ periods at incident angle $(\theta_0)=65°$ loaded with all samples one by one with respect to normal skin sample, efforts have been given to compare the performance of our structure with the performance of similar kind of works carried out earlier. This comparison is presented in Table 3 below.

Chen et al. demonstrated that the structure with two tangent air holes can be used as a gas sensor with sensitivity 353 nm/RIU and Q-factor 3.8×10^3[29]. L. heureux et al. reported distributed Bragg reflector having metal/nano porous GaN cavities. This structure works on Tamm plasmon resonance and it has sensitivity of 10 nm/RIU with Q-factor 300[30]. On the other hand, Klimov et at. studied photonic crystal structure perforated with gold film for biosensing application based on Fano resonances whose sensitivity was only limited to 17 nm/RIU with a Q-factor value of 3000[31]. Gao et al. investigated suspended slotted photonic crystal cavities for high-sensitivity refractive index sensing applications with sensitivity of 656 nm/RIU and Q-factor value of 2719[32]. Almawgani et al. suggested a theoretical approach for designing of an ultrasensitive SPR sensor which could sense sample of RI variation limited between 1.33 and 1.34[33]. Elsayed et al. suggested hybrid angular plasmonic sensor consisted of 2D material for detection of samples whose RI variation is limited between 1.330 and 1.340 and found the sensitivity of 488.2 °/RIU with a Q factor value of 2610.7[34]. Annular photonic biosensor for

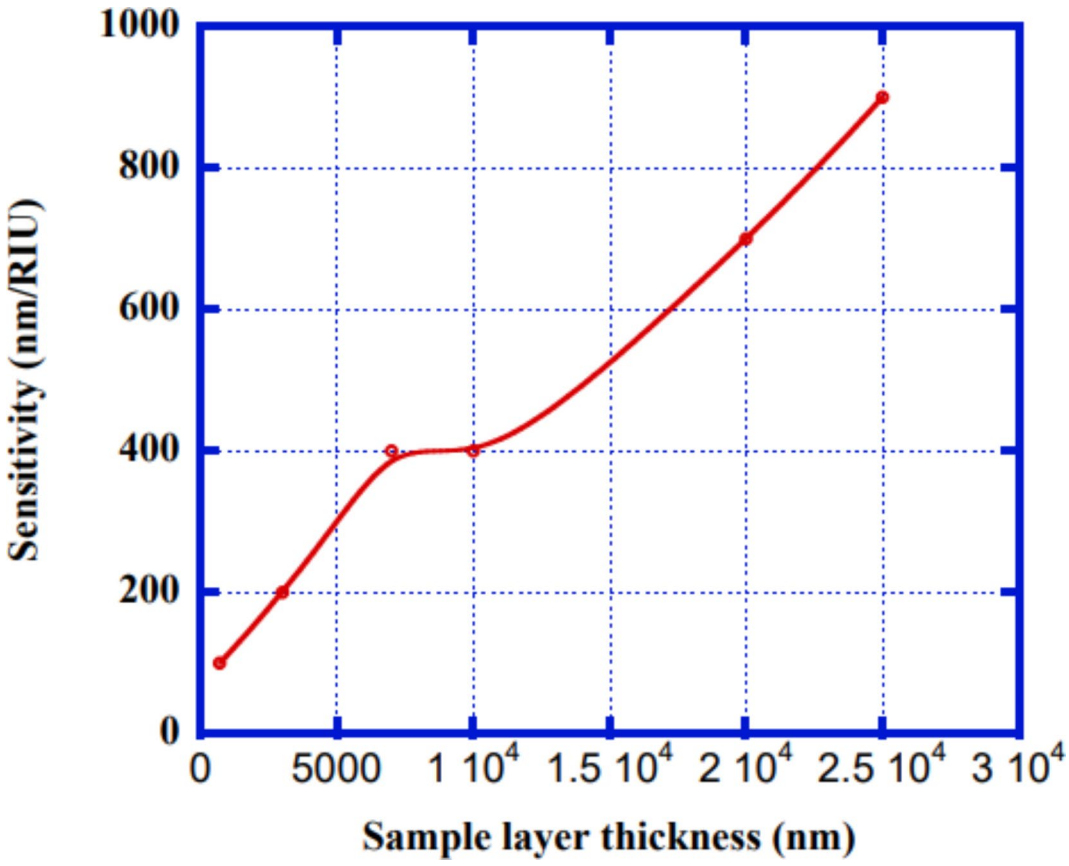

Fig. 10. Calculated sensitivity values of various structures of different cavity layer thickness loaded with sample containing dermis pigmentation with respect to normal sample.

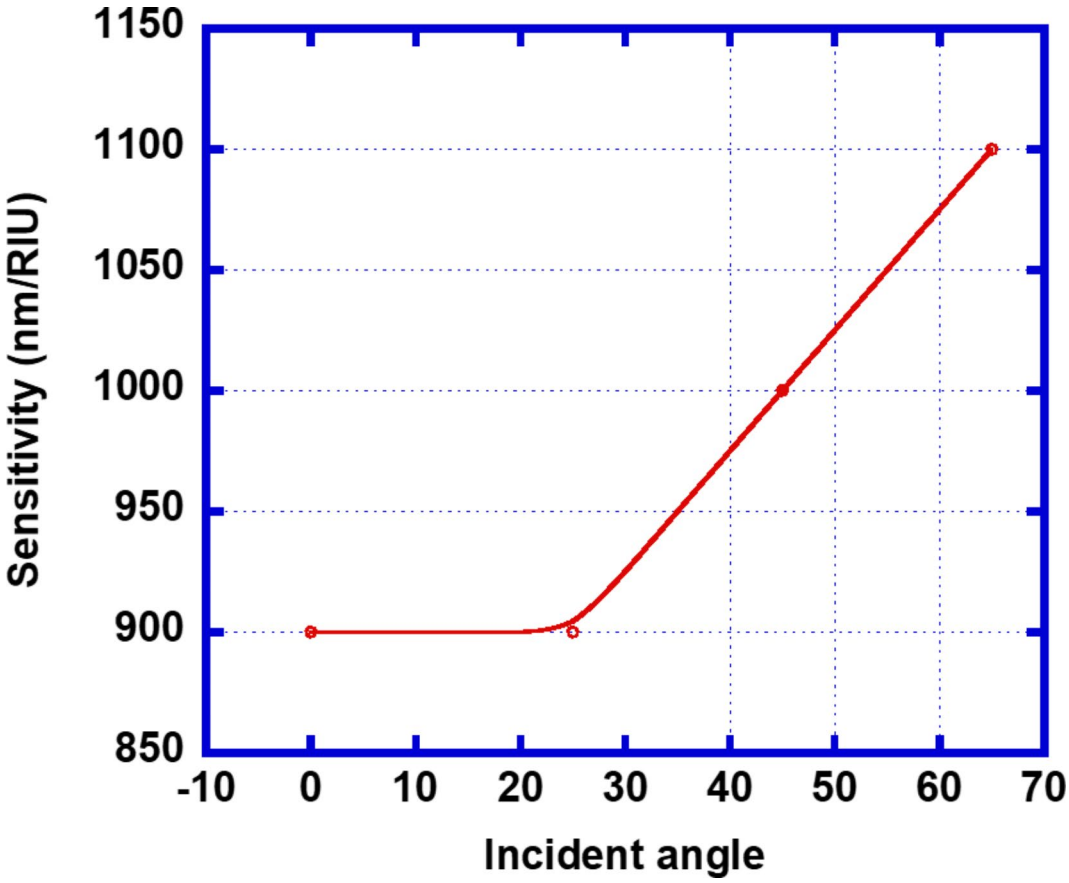

Fig. 11. Calculated sensitivity values of the structures of cavity layer thickness $d_{sm} = 25 \times 10^3$ nm loaded with sample containing dermis pigmentation with respect to normal sample under different angles of TE polarized light varying between 0˚ to 65˚.

Samples	RI (RIU)	Peak wavelength (nm)	Sensitivity (nm/RIU)	FWHM (nm)	Q-Factor
Normal skin	1.42	1614	---	0.05	32,280
Melanin	1.72	1671	190	0.05	33,420
Keratin	1.51	1630	177.7	0.04	40,750
Collagen	1.43	1626	1200	0.04	40,650
Dermis	1.41	1603	1100	0.06	26716.6
Epidermis	1.34	1579	437.5	0.05	31,580

Table 2. Numerically calculated values of sensitivity and Q-factor values of the structure having $d_{sm} = 25 \times 10^3$ nm and $N = 10$ periods at incident angle $(\theta_0) = 65°$ loaded with all samples one by one with respect to normal skin sample in addition to central wavelengths of various Tamm resonance peaks along with their FWHM.

protein detection is suggested by Sakshi et al. achieves the sensitivity of 576.27 nm/RIU with Q factor value of 5600[35].

Finally, It can be summarised from the data presented in Table 3 the proposed sensor can minutely detect vitiligo due to its maximum sensitivity values. The highest sensitivity which can be achieved by our structure is 1200 nm/RIU loaded with a sample containing collagen pigment with respect to normal sample. Moreover, our structure possesses exceptionally high Q factor value of 40,650 which makes our biosensing design most suitable for detecting vitiligo.

Conclusion

Highly sensitive planar photonic biosensor based on Tamm resonance capable of detecting of vitiligo is presented here. MATLAB simulations based on TMM are carried out for obtaining the results of the proposed theoretical research work. For excitation of Tamm plasmon polaritons the silver layer is attached with 1D PC via a hollow cavity region designed for loading various samples containing pigmented skin cells of melanin,

Reference	Sensitivity (nm/RIU)	Q-Factor
Ref[29]	353	3800
Ref[30]	10	300
Ref[31]	17	3000
Ref[32] Ref[33] Ref[34] Ref[35]	656 466 488.2 576.2	2719 375.8 2610.7 5600
Proposed work	1200	40,650

Table 3. Comparison of results of proposed work with the earlier work of others.

keratin, epidermis, collagen, and dermis separately one by one. The performance of the sensor loaded with various samples is evaluated by taking normal skin sample as a reference. Vitiligo is detected by measuring the change in the positions of TPR modes inside PBG of structure loaded with various pigments to conduct the desired analyses such as variation in transmittance, intensity and shift in position of Tamm resonant peak inside PBG under the influence of sample. Finally, our structure with $d_{sm} = 25 \times 10^3$ nm and $N = 10$ at angle of incidence 65° corresponding to TE polarization achieves sensitivity of 1200 nm/RIU under the influence of cavity containing collagen pigmentation with respect to the sample containing normal skin sample. Additionally, it finds exceptionally high Q factor value of 40,650. The present work may open new window for the development of other Tamm resonance based biosensing designs over convectional plasmonic SPR biosensors.

Data availability

The data that supports the findings of this study is available from the corresponding author upon reasonable request.

Received: 19 June 2024; Accepted: 16 December 2024
Published online: 06 January 2025

References

1. Spritz, R. A. The genetics of generalized vitiligo and associated autoimmune diseases. *Pigment Cell Res.* **20**, 271–278. https://doi.org/10.1111/j.1600-0749.2007.00384.x (2007).
2. Moretti, S., Amato, L., Bellandi, S. & Fabbri, P. Focus on Vitiligo: a generalized skin disorder. *Eur. J. Inflamm.* **4** (1), 21–30. https://doi.org/10.1177/1721727X0600400103 (2006).
3. Kovacs, D., Bastonini, E. & Ottaviani, M. & et al.Vitiligo skin: exploring the dermal compartment. *J. Invest. Dermatology Volume* **138**, Issue 2, 2018,Pages 394–404,ISSN 0022-202X, https://doi.org/10.1016/j.jid.2017.06.033
4. Nandhini, V. L., Babu, K. S., Sharan, A. & Venugopal, K. R. Detection of Vitiligo using Waveguide Resonator based on Optical Sensor, 2020 7th International Conference on Computing for Sustainable Global Development (INDIACom), New Delhi, India, 2020,. 192–197, https://doi.org/10.23919/INDIACom49435.2020.9083692
5. Mankotia, A. & Shukla, A. K. Detection of Vitiligo using Optical Sensor based on 2-D photonic crystals. *J. Phys. : Conf. Ser.* **2426**, 012020. https://doi.org/10.1088/1742-6596/2426/1/012020 (2023).
6. Smirnov, J. R. C., Calvo, M. E. & Míguez, H. Selective UV reflecting mirrors based on nanoparticle multilayers. *Adv. Funct. Mater.* **23**, 2805–2811. https://doi.org/10.1002/adfm.201202587 (2013).
7. Shaban, M. et al. Tunability and Sensing properties of Plasmonic/1D Photonic Crystal. *Sci. Rep.* **7**, 41983. https://doi.org/10.1038/srep41983 (2017).
8. Aly, A. H. & Elsayed, H. A. Defect mode properties in a one-dimensional photonic crystal. *Phys. B: Condens. Matter Volume*. **407** (Issue 1). https://doi.org/10.1016/j.physb.2011.09.137 (2012). Pages 120–125, ISSN 0921–4526.
9. Aly, A. H. et al. MATLAB simulation based study on poliovirus sensing through one-dimensional photonic crystal with defect. *Sci. Rep.* **13**, 9422. https://doi.org/10.1038/s41598-023-35595-6 (2023).
10. Aly, A. H. et al. A temperature sensor based on Si/PS/SiO2 photonic crystals. *Sci. Rep.* **13**, 21560. https://doi.org/10.1038/s41598-023-48836-5 (2023).
11. Aly, A. H. et al. Ultra-high sensitive cancerous cells detection and sensing capabilities of photonic biosensor. *Sci. Rep.* **13**, 19524. https://doi.org/10.1038/s41598-023-46667-y (2023).
12. Aly, A. H. et al. Ultra-sensitive pressure sensing capabilities of defective one-dimensional photonic crystal. *Sci. Rep.* **13**, 18876. https://doi.org/10.1038/s41598-023-45680-5 (2023).
13. Kushwaha, A. S., Kumar, A., Kumar, R. & Srivastava, S. K. A study of surface plasmon resonance (SPR) based biosensor with improved sensitivity, Photonics and nanostructures - fundamentals and Applications, **31**, Pages 99–106, ISSN 1569–4410, (2018). https://doi.org/10.1016/j.photonics.2018.06.003
14. Abinash Panda, A. & Pukhrambam, P. D. Design and modelling of reconfigurable surface plasmon resonance refractive index sensor employing graphene and Sb2S3 for detection of dengue virus. *Phys. B: Condens. Matter*. **638**, 0921–4526. https://doi.org/10.1016/j.physb.2022.413965 (2022).
15. Zaky, Z. A. & Aly, A. H. Highly sensitive salinity and temperature sensor using Tamm Resonance. *Plasmonics* **16**, 2315–2325. https://doi.org/10.1007/s11468-021-01487-6 (2021).
16. Zaky, Z. A. et al. Theoretical evaluation of the refractive index sensing capability using the coupling of Tamm–Fano resonance in one-dimensional photonic crystals. *Appl. Nanosci.* **11**, 2261–2270. https://doi.org/10.1007/s13204-021-01965-7 (2021).
17. -Huang, M. Stress effects on the performance of optical waveguides, International Journal of Solids and Structures, Volume 40, Issue 7, Pages 1615–1632, ISSN 0020-7683, (2003). https://doi.org/10.1016/S0020-7683(03)00037-4
18. Sohn, H. Refractive Index of Porous Silicon. doi: (2014). https://doi.org/10.1007/978-3-319-04508-5_25-1
19. Sharma, A. K. & Pandey, A. K. Blue Phosphorene/MoS2 Heterostructure Based SPR Sensor With Enhanced Sensitivity, in IEEE Photonics Technology Letters, vol. 30, no. 7, pp. 595–598, 1 April1, doi: (2018). https://doi.org/10.1109/LPT.2018.2803747
20. Pal, A. & Jha, A. A theoretical analysis on sensitivity improvement of an SPR refractive index sensor with graphene and barium titanate nanosheets, Optik, 231, 2021,166378, ISSN 0030-4026, https://doi.org/10.1016/j.ijleo.2021.166378

21. El-Khozondar, H. J. et al. N.R. &. Design of one dimensional refractive index sensor using ternary photonic crystal waveguide for plasma blood samples applications, Physica E: Low-dimensional Systems and Nano structures, Volume 111, Pages 29–36, ISSN 1386–9477, (2019). https://doi.org/10.1016/j.physe.2019.02.030
22. Abderrahmane, A., Senouci, K., Hachemi, B. & Ko, P. J. 2D Gallium Sulfide-based 1D Photonic Crystal Biosensor for glucose concentration detection. *Materials* **16** (13), 4621. https://doi.org/10.3390/ma16134621 (2023).
23. Daher, M. G., Jaroszewicz, Z. & Zyoud, S. H. Design of a novel detector based on photonic crystal nanostructure for ultra-high performance detection of cells with diabetes. *Opt. Quant. Electron.* **54**, 701. https://doi.org/10.1007/s11082-022-04093-w (2022).
24. Efimov, I. M., Vanyushkin, N. A. & Gevorgyan, A. H. The determination of the sensitivity of refractive index sensors. *Photonics* **11**, 56. https://doi.org/10.3390/photonics11010056 (2024).
25. Aly, A. H., Awasthi, S. K., Mohaseb, M. A., Matar, Z. S. & Amin, A. F. MATLAB Simulation-based theoretical study for detection of a wide range of pathogens using 1D defective Photonic structure. *Crystals* **12**, 220. https://doi.org/10.3390/cryst12020220 (2022).
26. Sampath, D. & Narasimhan, V. One-dimensional defect layer Photonic Crystal Sensor for Purity Assessment of Organic solvents. *ACS Omega*. **9** (8), 9625–9632. https://doi.org/10.1021/acsomega.3c09589 (2024).
27. Taya, S. A. et al. Sensitivity enhancement of an optical sensor based on a binary photonic crystal for the detection of Escherichia coli by controlling the central wavelength and the angle of incidence. *Opt. Quant. Electron.* **54**, 127. https://doi.org/10.1007/s11082-022-03511-3 (2022).
28. Abohassan, K. M., Ashour, H. S. & Abadla, M. M. A 1D photonic crystal-based sensor for detection of cancerous blood cells. *Opt. Quant. Electron.* **53**, 356. https://doi.org/10.1007/s11082-021-03014-7 (2021).
29. Chen, Z. H., Li, W., Han, Y., Jiang, H. & Hamamoto, K. Proposal of two tangent air hole structure for higher sensitivity gas sensor. *Japan J. Appl. Phys.* **58**, SJJD03. https://doi.org/10.7567/1347-4065/ab26ab (2019).
30. Lheureux, G. et al. Tamm plasmons in metal/nanoporous GaN distributed Bragg reflector cavities for active and passive optoelectronics. *Opt. Expr.* **28** (12), 17934–17943 (2020).
31. Klimov, V. V., Pavlov, A. A., Treshin, I. V. & Zabkov, I. V. Fano resonances in a photonic crystal covered with a perforated gold film and its application to bio-sensing. *J. Phys. D-Appl Phys.* **50** (28), 285101 (2017).
32. Gao, Y., Dong, P. & Shi, Y. Suspended slotted photonic crystal cavities for high-sensitivity refractive index sensing. *Opt. Expr.* **28** (8), 12272–12278 (2020).
33. Almawgani, A. H. M. et al. A theoretical approach for a new design of an ultrasensitive angular plasmonic chemical sensor using black phosphorus and aluminum oxide architecture. *RSC Adv.* **13** (24), 16154–16164. https://doi.org/10.1039/D3RA01984E (2023).
34. Elsayed, H. A. et al. High-performance biosensors based on angular plasmonic of a multilayer design: new materials for enhancing sensitivity of one-dimensional designs. *RSC Adv.* **14** (11), 7877–7890. https://doi.org/10.1039/D3RA08731J (2024).
35. Gandhi, S. & Awasthi, S. K. Protein detection capabilities of photonic biosensor composed of 1D annular photonic crystal. *Results Opt.* **15**, 100639. https://doi.org/10.1016/j.rio.2024.100639 (2024).

Acknowledgements

The authors extend their appreciation to the Deanship of Research and Graduate Studies at King Khalid University for funding this work through Large Research Project under grant number R.G.P. 2/77/45.

Author contributions

B.A.M., D.M., S.A., S.K.A., A.F.A., A.S.A., H.H., Z.M. and A. H. A. conceived of the presented idea and developed the theory. A.H.A., B.A.M. and D.M. performed the computations. D.M., B.A.M. wrote the manuscript with support from S.K.A and A. H.A. In addition, A. H.A. supervised this work. All authors discussed the results and contributed to the final manuscript.

Declarations

Competing interests

The authors declare no competing interests.

Additional information

Correspondence and requests for materials should be addressed to A.H.A.

Reprints and permissions information is available at www.nature.com/reprints.

Publisher's note Springer Nature remains neutral with regard to jurisdictional claims in published maps and institutional affiliations.